Available online at www.sciencedirect.com
SCIENCE DIRECT®
Journal of Magnetic Resonance 165 (2003) 80–88
JMR Journal of Magnetic Resonance
www.elsevier.com/locate/jmr

# Frequency-domain method based on the singular value decomposition for frequency-selective NMR spectroscopy☆

Petre Stoica,[a] Niclas Sandgren,[a,*] Yngve Selén,[a] Leentje Vanhamme,[b] and Sabine Van Huffel[b]

[a] *Systems and Control Division, Department of Information Technology, Uppsala University, P.O. Box 337, SE-751 05 Uppsala, Sweden*
[b] *Department of Electrical Engineering (ESAT), Katholieke Universiteit Leuven, Kasteelpark Arenberg 10, 3001 Leuven, Belgium*

Received 24 April 2003; revised 22 May 2003

**Abstract**

In several applications of NMR spectroscopy the user is interested only in the components lying in a small frequency band of the spectrum. A frequency selective analysis deals precisely with this kind of NMR spectroscopy: parameter estimation of only those spectroscopic components that lie in a preselected frequency band of the NMR data spectrum, with as little interference as possible from the out-of-band components and in a computationally efficient way. In this paper we introduce a frequency-domain singular value decomposition (SVD)-based method for frequency selective spectroscopy that is computationally simple, statistically accurate, and which has a firm theoretical basis. To illustrate the good performance of the proposed method we present a number of numerical examples for both simulated and in vitro NMR data.


*Keywords:* Frequency-selective spectroscopy; Frequency-domain data processing; SVD-based parameter estimation; Damped sinusoidal model; In vitro data analysis

## 1. Introduction and problem formulation

We consider the following model commonly used for NMR data:

$$y(t) = \sum_{k=1}^{m} \rho_k \lambda_k^t + \epsilon(t), \quad \lambda_k = \mathrm{e}^{-\alpha_k + \mathrm{i}\omega_k}, \quad t = 0, \ldots, N-1 \tag{1}$$

where $m$ denotes the number of components, $(\rho_k, \alpha_k, \omega_k)$ are the complex amplitude, damping and frequency of the $k$th component (note that the sampling period has been absorbed in $\alpha_k$ and $\omega_k$, for notational convenience), $\epsilon(t)$ is a noise term and $N$ denotes the number of available samples. Both $m$ and $(\rho_k, \alpha_k, \omega_k)$ are unknown.

In some applications, such as metabolite imaging, it would be too computationally intensive to estimate the parameters of all components in Eq. (1). For this and other reasons (see point (ii) below) we may be interested in only a few components of Eq. (1) that lie in a prespecified frequency band comprising the following Fourier frequencies:

$$\left\{ \frac{2\pi k_1}{N}, \frac{2\pi k_2}{N}, \ldots, \frac{2\pi k_M}{N} \right\}. \tag{2}$$

Here $k_1, \ldots, k_M$ are $M$ given integers. Usually $k_1, \ldots, k_M$ are consecutive integers ($k_2 = k_1 + 1$, $k_3 = k_2 + 1$, etc.), however the method developed in the following does not require them to be so and hence it can be applied even when the interval in Eq. (2) contains several *non-adjacent* frequency bands. We assume that the number of components of Eq. (1) lying in the frequency band of Eq. (2), which we denote by

$$n \leqslant m \tag{3}$$

is given. If $n$ was a priori unknown, it could be estimated from the data either by counting the peaks of the spectrum of Eq. (1) that lie in the frequency band of Eq. (2) or as the rank of a certain data matrix that will be introduced later on (see Section 2).

☆ This work was partly supported by the Swedish Science Council.
* Corresponding author. Fax: +46-18-503611.
*E-mail address:* niclas.sandgren@it.uu.se (N. Sandgren).

1090-7807/$ - see front matter © 2003 Elsevier Inc. All rights reserved.
doi:10.1016/S1090-7807(03)00188-5

Our problem therefore is to estimate the parameters of the ($n$) components of Eq. (1) that lie in the frequency band in Eq. (2). Furthermore, we want to find a solution to this frequency-selective estimation problem that has the following properties.

(i) *It is computationally efficient*. In particular, the computational complexity of such a solution should be comparable with that of a standard SVD-based method applied to a data model having the form of Eq. (1) but with $m = n$ and $N = M$.

(ii) *It is statistically accurate*. To be more specific about this aspect we will split the discussion in two parts. From a theoretical standpoint, estimating $n < m$ components of Eq. (1) (in the presence of the remaining components and noise) cannot produce more accurate estimates than estimating all $m$ components. Even so, for a good frequency-selective method the aforementioned degradation of the theoretical statistical accuracy should not be significant. On the other hand, from a practical standpoint, a sound frequency-selective method may give better performance than a non-frequency-selective counterpart that deals with all components in Eq. (1). This is so because some components in Eq. (1) that do not belong to Eq. (2) (such as the solvent) may not be well described by a damped sinusoid model; consequently treating such components as uninteresting interferences and eliminating them from the model (see the next section) may improve the estimation accuracy of the components of interest. In addition, for a subspace based method, when prior knowledge is available about the components of interest, this can be more easily taken into consideration (to enhance the estimation accuracy) in an approach that eliminates the nuisance components from the model and deals only with the components of interest (see, e.g., [1,2]).

In the next section we introduce a frequency-selective SVD-based method that possesses the above two desirable features. Several methods have been developed in the past for frequency-selective parameter estimation (see, e.g., [3–8,15,16] and the references therein). Of the cited methods, the so-called filter diagonalization method (FDM) of [15,16] is the closest in spirit to the method proposed in the present paper. As shown in the next section our proposed method can be viewed as a frequency-domain implementation of ESPRIT (see, e.g., [10]). Somewhat similarly, FDM can be viewed as a frequency-domain implementation of the related state-space and matrix pencil methods of spectral analysis, which are well known in the signal processing community (see, e.g., [17–19]). We leave a detailed comparison between FDM and the method proposed herein for a future paper.

In Section 2 we develop a frequency-domain SVD-based method that is computationally simple, statistically accurate and has a sound theoretical basis. In Section 3 we present a number of numerical examples to illustrate the type of performance that can be achieved by using our approach. We will compare the performance of our frequency-selective method with that of the method in [6].

## 2. Frequency-domain SVD-based method

The main source of inspiration for our frequency-domain SVD-based approach, which we will designate by the acronym SELF-SVD (the abbreviation SELF indicates the fact that the method is usable in a **sel**ected **f**requency band), was [9] where a frequency-domain method for *un*damped sinusoidal models was proposed. However, the derivation of SELF-SVD presented in what follows (for the more general case of the damped sinusoids-in-noise model in Eq. (1)) is simpler and more self-contained than that in [9].

The following notation will be frequently used in the paper:

$$w_k = \mathrm{e}^{\mathrm{i}2\pi k/N}, \quad k = 0, \ldots, N-1, \tag{4}$$

$$\mathbf{u}_k = [w_k \cdots w_k^S]^{\mathrm{T}}, \tag{5}$$

$$\mathbf{v}_k = [1 w_k \cdots w_k^{N-1}]^{\mathrm{T}} \quad (\text{the } k\text{th Fourier vector}), \tag{6}$$

$$\mathbf{y} = [y(0) \cdots y(N-1)]^{\mathrm{T}} \quad (\text{the data vector}), \tag{7}$$

$$Y_k = \mathbf{v}_k^* \mathbf{y} \quad k = 0, \ldots, N-1 \quad (\text{the FFT sequence}), \tag{8}$$

$$\mathbf{a}(\lambda_k) = [\lambda_k \cdots \lambda_k^S]^{\mathrm{T}}, \tag{9}$$

$$\mathbf{b}(\lambda_k) = [1 \lambda_k \cdots \lambda_k^{N-1}]^{\mathrm{T}} \tag{10}$$

(the Vandermonde vector associated with the $k$th mode).

Hereafter $S$ is a user parameter whose choice is discussed later on, and $*$ denotes the conjugate transpose. In Appendix A we show that the following key equation involving the frequency-domain data $\{Y_k\}$ holds true:

$$\mathbf{u}_k Y_k = [\mathbf{a}(\lambda_1) \cdots \mathbf{a}(\lambda_m)] \begin{bmatrix} \rho_1 \mathbf{v}_k^* \mathbf{b}(\lambda_1) \\ \vdots \\ \rho_m \mathbf{v}_k^* \mathbf{b}(\lambda_m) \end{bmatrix} + \mathbf{\Gamma} \mathbf{u}_k + \mathbf{u}_k \varepsilon_k, \tag{11}$$

where $\{\varepsilon_k\}$ is similarly defined to $\{Y_k\}$, that is the sequence $\{\varepsilon_k\}$ is the FFT of the noise $\{\epsilon(t)\}_{t=0}^{N-1}$, and $\mathbf{\Gamma}$ is an $S \times S$ matrix defined in Eq. (A.6) of Appendix A (the definition of $\mathbf{\Gamma}$ is not repeated here because it has no importance for what follows, as will become clear shortly).

In the following we let $\{\lambda_k\}_{k=1}^n$ denote the modes of Eq. (1) whose frequencies lie in Eq. (2). To separate the terms in Eq. (11) corresponding to the modes of interest

from those associated with the nuisance modes we make use of the following notation:

$$\mathbf{A} = [\mathbf{a}(\lambda_1) \cdots \mathbf{a}(\lambda_n)], \tag{12}$$

$$\mathbf{x}_k = \begin{bmatrix} \rho_1 \mathbf{v}_k^* \mathbf{b}(\lambda_1) \\ \vdots \\ \rho_n \mathbf{v}_k^* \mathbf{b}(\lambda_n) \end{bmatrix} \tag{13}$$

for the modes of interest whose frequencies belong to the interval in Eq. (2), and similarly $\tilde{\mathbf{A}}$ and $\tilde{\mathbf{x}}_k$ for the other modes. Finally, to write Eq. (11) for $k = k_1, \ldots, k_M$ in a compact matrix form we need the following additional notation:

$$\mathbf{Y} = [\mathbf{u}_{k_1} Y_{k_1} \cdots \mathbf{u}_{k_M} Y_{k_M}], \tag{14}$$

$$\mathbf{U} = [\mathbf{u}_{k_1} \cdots \mathbf{u}_{k_M}], \tag{15}$$

$$\mathbf{X} = [\mathbf{x}_{k_1} \cdots \mathbf{x}_{k_M}], \tag{16}$$

and similarly for $\tilde{\mathbf{X}}$. Using this notation, we can write Eq. (11) (for $k = k_1, \ldots, k_M$) as follows:

$$\mathbf{Y} = \mathbf{A}\mathbf{X} + \mathbf{\Gamma}\mathbf{U} + \tilde{\mathbf{A}}\tilde{\mathbf{X}} + \boldsymbol{\varepsilon}, \tag{17}$$

where the $S \times M$ matrix $\boldsymbol{\varepsilon}$ is defined similarly to $\mathbf{Y}$.

Next we assume that:

$$M \geqslant n + S, \tag{18}$$

which does not introduce any restriction, as the user parameter $S$ can always be chosen to satisfy Eq. (18) (the choice of $S$ is discussed later on in this section). Under Eq. (18) (in fact only $M \geqslant S$ is required for this part), the orthogonal projection matrix onto the null space of $\mathbf{U}$ is given by

$$\mathbf{\Pi}_U^{\perp} = \mathbf{I} - \mathbf{U}^*(\mathbf{U}\mathbf{U}^*)^{-1}\mathbf{U}. \tag{19}$$

We will eliminate the second term in Eq. (17) by post-multiplying this equation with $\mathbf{\Pi}_U^{\perp}$ (see below). However, before doing so we make the following observations about the third and fourth terms in Eq. (17).

(a) The elements of the noise term are much smaller than the elements of $\mathbf{AX}$. Indeed, it can be shown that $\varepsilon_k = \mathcal{O}(N^{1/2})$ (stochastically), whereas the order of the elements of $\mathbf{X}$ is typically $\mathcal{O}(N)$ (note that for this to hold the signal-to-noise ratio in the raw data, see Eq. (1), need not be high).

(b) Similarly, assuming that the out-of-band components are not much stronger than the components in the band of interest and that the frequencies of the former are not too close to the interval in Eq. (2), the elements of $\tilde{\mathbf{X}}$ are much smaller than the elements of $\mathbf{X}$.

(c) To understand what happens in the case that the assumption we made in (b) above does not hold, let us consider a generic out-of-band component $(\rho, \lambda)$. The part of $\mathbf{y}$ corresponding to such a component can be written as $\rho\, \mathbf{b}(\lambda)$. Hence the corresponding part in $\mathbf{u}_k Y_k$ is given by $\rho\, \mathbf{u}_k[\mathbf{v}_k^* \mathbf{b}(\lambda)]$ and, consequently, the part of $\mathbf{Y}$ due to this generic component would be

$$\rho \mathbf{U} \begin{bmatrix} \mathbf{v}_{k_1}^* \mathbf{b}(\lambda) & & 0 \\ & \ddots & \\ 0 & & \mathbf{v}_{k_M}^* \mathbf{b}(\lambda) \end{bmatrix}. \tag{20}$$

Even if the frequency of $\lambda$ is relatively close to the band of interest in Eq. (1), we may expect that $\mathbf{v}_k^* \mathbf{b}(\lambda)$ does not vary significantly for $k \in [k_1, k_M]$ (in other words, the "spectral tail" of the out-of-band component may well have a small dynamic range in the interval of interest). As a consequence, the matrix in Eq. (20) is approximately proportional to $\mathbf{U}$ and hence it will be attenuated via the post-multiplication of it by $\mathbf{\Pi}_U^{\perp}$ (see below). A similar argument shows that the noise term in Eq. (17) also is attenuated by the post-multiplication of Eq. (17) with $\mathbf{\Pi}_U^{\perp}$.

It follows from the previous discussion (see Eq. (17) and (a)–(c) above) that

$$\mathbf{Y}\mathbf{\Pi}_U^{\perp} \approx \mathbf{A}\mathbf{X}\mathbf{\Pi}_U^{\perp}. \tag{21}$$

Under Eq. (18) and some additional "regularity" conditions it can be shown that (see [9] and references therein for a proof of this type of result):

$$\operatorname{rank}(\mathbf{X}\mathbf{\Pi}_U^{\perp}) = n. \tag{22}$$

Hence, assuming that

$$S \geqslant n \tag{23}$$

(which is an easily satisfied condition), we have from Eqs. (21) and (22) that:

$$\operatorname{effrank}(\mathbf{Y}\mathbf{\Pi}_U^{\perp}) = n \tag{24}$$

and

$$\mathbf{A} \approx \mathbf{W}\mathbf{P}, \tag{25}$$

where effrank stands for effective rank,

$$\mathbf{W} = \text{the } S \times n \text{ matrix whose columns are the left singular vectors of } \mathbf{Y}\mathbf{\Pi}_U^{\perp} \text{ associated with the } n \text{ largest singular values} \tag{26}$$

and $\mathbf{P}$ is a nonsingular transformation matrix.

Our proposal for a frequency-selective spectroscopic method relies on the results of Eqs. (24) and (25) above: using Eq. (24) we can estimate $n$ or, at least, verify an assumed value for $n$; whereas using Eq. (25) we can estimate the modes of interest $\{\lambda_k\}_{k=1}^n$ via a standard SVD-based method (see, e.g., [10]); finally, once $\{\lambda_k\}$ have been estimated we can estimate $\{\rho_k\}_{k=1}^n$ (see below). The steps of the proposed method are described in more detail in the following.

*SELF-SVD method for frequency-selective NMR spectroscopy*

*Step 1.* Apply an FFT algorithm to $\{y(t)\}_{t=0}^{N-1}$ to compute $\{Y_k\}_{k=0}^{N-1}$. Determine the frequency band of interest $[2\pi k_1/N, 2\pi k_M/N]$ by the inspection of $\{Y_k\}$ (possibly the band of interest is pre-specified), as well as the value of $n$ (possibly $n$ can also be pre-specified).

Choose $S$ in the interval:

$$S \in \left[\left\lceil \frac{M}{3} \right\rceil, \left\lceil \frac{M}{2} \right\rceil\right], \tag{27}$$

where $\lceil x \rceil$ denotes the integer part of $x$. This interval for $S$ is suggested by the previous experience with SVD-based approaches (see, e.g., [10]) as well as our empirical experience with SELF-SVD. In the numerical examples we will use the lower limit in Eq. (27), viz., $S = \lceil M/3 \rceil$, to reduce the computational burden of SELF-SVD.

*Step 2.* Compute $\mathbf{\Pi}_U^{\perp}$; this can be conveniently done using the QR decomposition of $\mathbf{U}^*$,

$$\mathbf{U}^* = [\underbrace{\overline{\mathbf{Q}}}_{S} \underbrace{\mathbf{Q}}_{M-S}] \begin{bmatrix} \mathbf{R} \\ 0 \end{bmatrix}^{\}S}; \quad \mathbf{Q}^*\mathbf{Q} = \mathbf{I}_{M-S}, \tag{28}$$

which gives

$$\mathbf{\Pi}_U^{\perp} = \mathbf{Q}\mathbf{Q}^*. \tag{29}$$

Next compute the matrix

$$\mathbf{Z} = \mathbf{Y}\mathbf{\Pi}_U^{\perp} \tag{30}$$

and its singular value decomposition. Check (by the inspection of the singular values) that the effective rank of $\mathbf{Z}$ is equal to the value of $n$ given by Step 1 (otherwise adjust $n$ accordingly). Build the $S \times n$ matrix $\mathbf{W}$ from the left singular vectors of $\mathbf{Z}$ associated with the $n$ largest singular values.

*Step 3.* Estimate $\{\lambda_k\}_{k=1}^n$ from $\mathbf{W}$ by a standard SVD method. We present a succinct derivation of such an SVD-based method, for the reader less familiar with the SVD approach. Let

$$\mathbf{W}_u = [\mathbf{I}_{S-1}\ 0]\mathbf{W}, \tag{31}$$

$$\mathbf{W}_l = [0\ \mathbf{I}_{S-1}]\mathbf{W}, \tag{32}$$

and similarly for $\mathbf{A}$. Observe from Eq. (25) that

$$\mathbf{W}_l\mathbf{P} \approx \mathbf{A}_l = \mathbf{A}_u \begin{bmatrix} \lambda_1 & & 0 \\ & \ddots & \\ 0 & & \lambda_n \end{bmatrix} \approx \mathbf{W}_u\mathbf{P} \begin{bmatrix} \lambda_1 & & 0 \\ & \ddots & \\ 0 & & \lambda_n \end{bmatrix} \tag{33}$$

or, equivalently,

$$\mathbf{W}_l \approx \mathbf{W}_u\mathbf{\Phi}, \tag{34}$$

where

$$\mathbf{\Phi} = \mathbf{P} \begin{bmatrix} \lambda_1 & & 0 \\ & \ddots & \\ 0 & & \lambda_n \end{bmatrix} \mathbf{P}^{-1}. \tag{35}$$

Consequently, we can estimate $\mathbf{\Phi}$ from Eq. (34) by the least squares (LS) method:

$$\hat{\mathbf{\Phi}} = (\mathbf{W}_u^*\mathbf{W}_u)^{-1}\mathbf{W}_u^*\mathbf{W}_l \tag{36}$$

(alternatively we can use the total LS method (see, e.g., [11]) to estimate $\mathbf{\Phi}$), and then estimate $\{\lambda_k\}_{k=1}^n$ as the eigenvalues of $\hat{\mathbf{\Phi}}$ (note from Eq. (35) that the eigenvalues of $\mathbf{\Phi}$ are precisely given by $\{\lambda_k\}_{k=1}^n$).

*Step 4.* Finally, we use the estimates of $\{\lambda_k\}$ obtained in the previous step and the APES method of [12] to estimate $\{\rho_k\}_{k=1}^n$ (the acronym APES stands for **a**mplitude and **p**hase **es**timation). Note that there are several other methods that could be used for amplitude estimation, once $\{\lambda_k\}$ have been estimated. Our choice of APES is motivated by the fact that this method typically provides the most accurate amplitude estimates of all methods of which we are aware, at a reasonable computational cost (see, e.g., [14]). In what follows, we present a brief review of APES for the reader's convenience.

Let

$$\mathbf{z}(t) = [y(t) \cdots y(t+P-1)]^{\mathrm{T}}, \quad t = 0, 1, \ldots, L-1, \tag{37}$$

where $P > 1$ is a user parameter (the choice of which will be discussed in Section 3), and

$$L = N - P + 1. \tag{38}$$

Also, let $\mathbf{h}(\alpha, \omega) \in \mathcal{C}^{P\times 1}$ denote the coefficient vector of an FIR filter (to be applied to $\{y(t)\}$) which is such that:

(C1) the damped sinusoid $\{\rho e^{(-\alpha+i\omega)t}\}$ passes undistorted through the filter; and

(C2) the filter output $\mathbf{h}^*(\alpha, \omega)\mathbf{z}(t)$ is as close as possible in the LS sense to a damped sinusoid with the given damping and frequency $(\alpha, \omega)$ and with an amplitude $(\rho)$ that minimizes the LS fitting error.

Let

$$\mathbf{s}(\alpha, \omega) = \left[1 e^{-\alpha+i\omega} \cdots e^{(-\alpha+i\omega)(P-1)}\right]^{\mathrm{T}}. \tag{39}$$

Condition C1 is satisfied if and only if

$$\mathbf{h}^*(\alpha, \omega)\mathbf{s}(\alpha, \omega) = 1. \tag{40}$$

Condition C2 is satisfied, for given $\alpha$ and $\omega$, by minimizing the following LS criterion (with respect to both $\mathbf{h}(\alpha, \omega)$ and $\rho$)

$$\sum_{t=1}^{L} \left|\mathbf{h}^*(\alpha, \omega)\mathbf{z}(t) - \rho e^{(-\alpha+i\omega)t}\right|^2 \tag{41}$$

subject to condition C1. The solution to Eq. (41) is given by (see [12] and references therein)

$$\hat{\rho}(\alpha,\omega) = \mathbf{h}^*(\alpha,\omega)\mathbf{Z}(\alpha,\omega), \tag{42}$$

where

$$\mathbf{Z}(\alpha,\omega) = \frac{1}{G(\alpha)}\sum_{t=1}^{L}[\mathbf{z}(t)\mathrm{e}^{-\alpha t}]\mathrm{e}^{-\mathrm{i}\omega t}, \tag{43}$$

$$G(\alpha) = \sum_{t=1}^{L}\mathrm{e}^{-2\alpha t} = \mathrm{e}^{-2\alpha}\frac{\mathrm{e}^{-2\alpha L}-1}{\mathrm{e}^{-2\alpha}-1}, \tag{44}$$

$$\mathbf{h}(\alpha,\omega) = \frac{\mathbf{Q}^{-1}(\alpha,\omega)\mathbf{s}(\alpha,\omega)}{\mathbf{s}^*(\alpha,\omega)\mathbf{Q}^{-1}(\alpha,\omega)\mathbf{s}(\alpha,\omega)}, \tag{45}$$

$$\mathbf{Q}(\alpha,\omega) = \mathbf{R} - G(\alpha)\mathbf{Z}(\alpha,\omega)\mathbf{Z}^*(\alpha,\omega), \tag{46}$$

$$\mathbf{R} = \sum_{t=1}^{L}\mathbf{z}(t)\mathbf{z}^*(t). \tag{47}$$

The computation of the amplitude estimate(s) in Eq. (42) concludes the description of the SELF-SVD algorithm.

To end this section we remark on the fact that the full-band SELF-SVD method, which uses $M = N$, can be shown to be equivalent to the standard time-domain SVD method applied to the usual $S \times (N - S)$ Hankel data matrix. In our opinion this is a desirable feature of any sound frequency-selective approach.

## 3. Numerical examples

### 3.1. Simulated data

The proposed SELF-SVD method will be compared to the frequency-selective ER-filter (ER stands for **e**xtraction and **r**eduction of the spectral bandwidth) method introduced in [6] and a standard time-domain SVD method (HSVD) (see e.g., [10,13]). HSVD will also be employed for the quantitation (i.e., parameter estimation) of the size-reduced data sequence after ER-filtering. The name we will use for the so-obtained frequency-selective method is ERF-HSVD. A two peak example is considered in detail to compare the estimation accuracy of the three methods, the sensitivity to the choice of frequency interval and the influence of a nuisance peak. The added noise is circular, white and Gaussian distributed with standard deviation $\sigma$. The quality of the different parameter estimates is measured as the relative root mean square error (RRMSE) for each peak $k = 1,\ldots,n$ [in percent]:

$$\mathrm{RRMSE}_k \triangleq 100\sqrt{\frac{1}{I}\sum_{l=1}^{I}\frac{(\xi_k - \hat{\xi}_k^l)^2}{\xi_k^2}}, \tag{48}$$

where $I$ is the number of Monte-Carlo runs (we used 1000 here), $\xi_k$ denotes the relevant parameter and $\hat{\xi}_k^l$ is its estimate obtained in the $l$th run.

Consider a data sequence consisting of two exponentially damped sinusoids of which only one (peak 1) is of interest. The two components have the following true parameter values (where au stands for amplitude units):

$$\omega_1 = 20\,\mathrm{Hz}, \quad \omega_2 = \text{varied},$$

$$\alpha_1 = 10\,\mathrm{Hz}, \quad \alpha_2 = 10\,\mathrm{Hz},$$

$$\rho_1 = 20\,\mathrm{au}, \quad \rho_2 = 320\,\mathrm{au}.$$

The sampling frequency ($f_s$) is 1 kHz and the number of data points $N$ is 512. Unless otherwise specified, the noise standard deviation used in these simulations ($\sigma$) is 5 and the frequency of peak 2 ($\omega_2$) is 100 Hz.

Throughout these simulations we consider two different frequency intervals. The first interval (Interval I) is small compared to $N$. The lower and upper frequency bounds (corresponding to $k_1$ and $k_M$) are set to 10 and 29 Hz, respectively. This interval was empirically found to be optimal for ERF-HSVD and it corresponds to about $\frac{1}{50}$ of the total number of data samples $N$ (i.e., $M = 11$ and $S = 3$ which satisfies Eqs. (18) and (23)). The transformation between $k$ and frequency $f$ in Hz is given by Eq. (49); note that $k$ is periodic in the same sense as the frequency:

$$\begin{aligned} k \leqslant \frac{N}{2} \;&\Rightarrow\; f = \frac{kf_s}{N}, \\ k > \frac{N}{2} \;&\Rightarrow\; f = \frac{-(N-k)f_s}{N}. \end{aligned} \tag{49}$$

The second interval considered (Interval II) is relatively large compared to $N$. The lower and upper frequency bounds are set to −141 and 78 Hz, respectively. This region was empirically found to be well suited for SELF-SVD and it corresponds to about $\frac{1}{5}$ of the total number of data samples (i.e., $M = 113$ and $S = 37$). The frequency bounds are preferably chosen so that as much as possible of the tails of the peak(s) of interest are included but without including nuisance peaks. If there is a "spectral gap" (meaning an interval including only noise with low spectral energy) between the region of interest and nuisance peaks, then this "gap" might be included in order to increase the estimation accuracy depending on whether the focus lies on parameter estimation accuracy or on computational simplicity. Later on we will show numerically that SELF-SVD, in contrast to ERF-HSVD, is not particularly sensitive to the choice of frequency interval. The RRMSEs Eq. (48) for the three parameters of interest ($|\rho_1|$, $\omega_1$, $\alpha_1$) corresponding to the two frequency intervals are shown in Figs. 1–3 for increasing noise standard deviation. In these figures, we see that there is a severe increase in the RRMSEs for HSVD when the signal is buried in heavy noise (i.e., a noise standard deviation above about 20). The reason for this was the occurrence of a noise peak, somewhere in the spectrum, with higher amplitude than

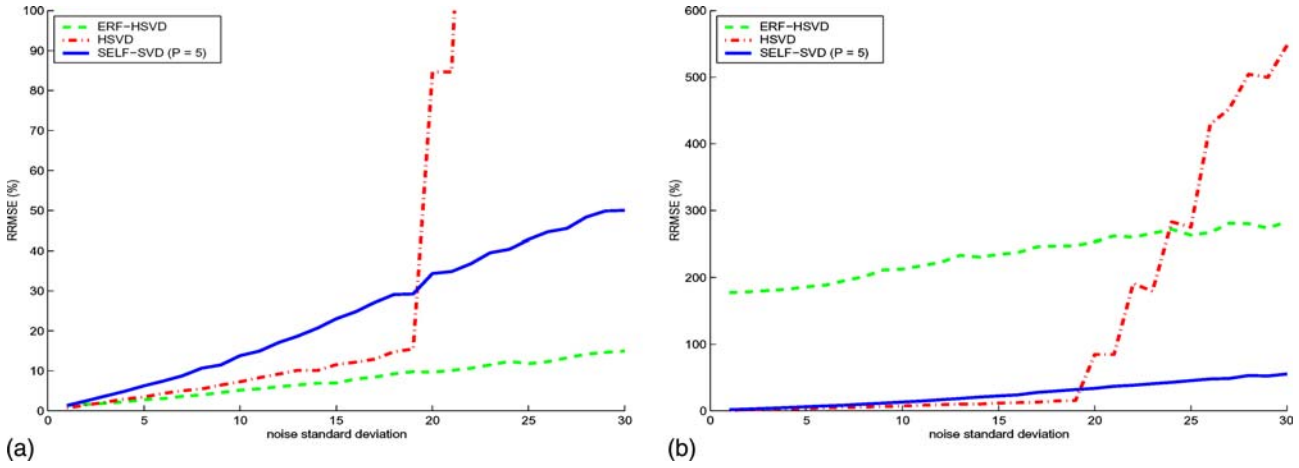


Fig. 1. Amplitude RRMSEs for peak 1 in the two-peak example: (a) Interval I; (b) Interval II.

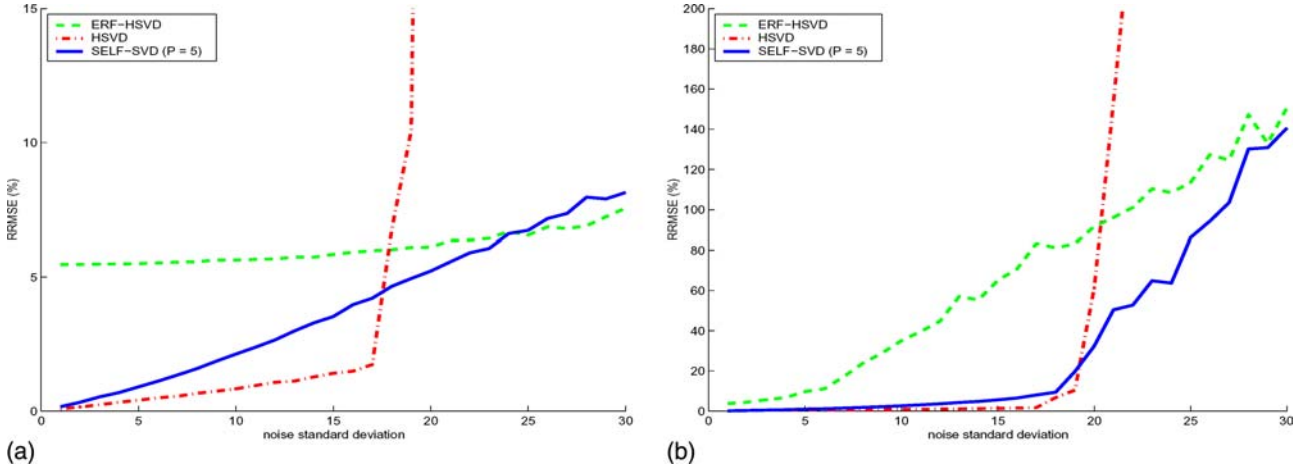


Fig. 2. Frequency RRMSEs for peak 1 in the two-peak example: (a) Interval I; (b) Interval II.

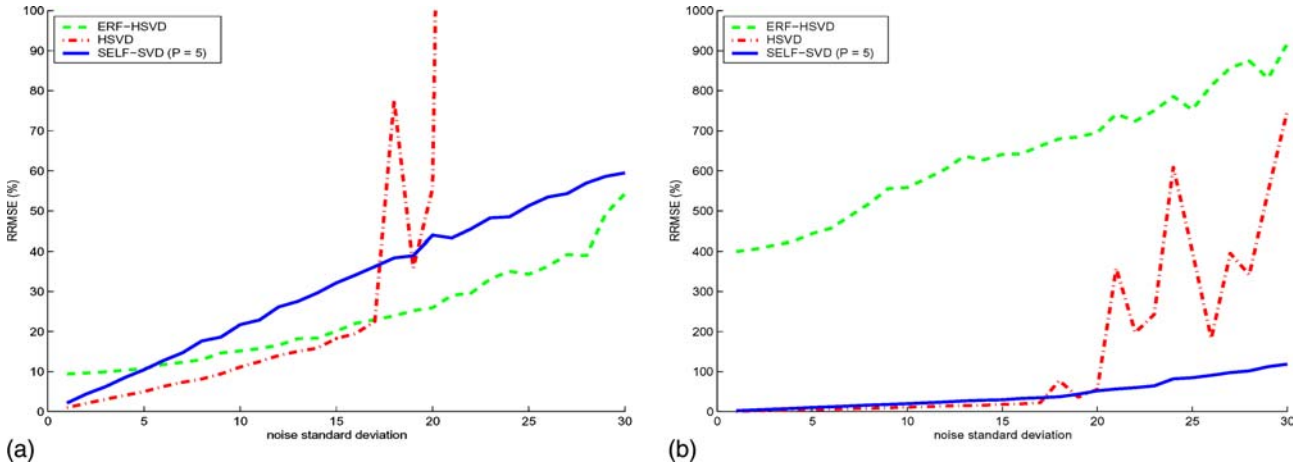


Fig. 3. Damping RRMSEs for peak 1 in the two-peak example: (a) Interval I; (b) Interval II.

peak 1 which led to a false peak estimate. This clearly motivates the use of a frequency selective method instead of a standard time-domain SVD method.

For data with few peaks a short FIR filter can be used for the amplitude estimation step in SELF-SVD (as described in Step 4). For more complex data the

selection of $P$ becomes a compromise between computational speed and estimation accuracy. Here we choose $P = \lceil N/100 \rceil$. The method is not particularly sensitive to the choice of $P$, but a short filter length results in reduced simulation times.

The computational speed of the two frequency selective methods is much superior to that of HSVD. Table 1 shows the required number of flops to perform one simulation run of each method. The magnitude of these values is of course dependent on the size of the frequency interval of interest, the number of peaks and the total number of data samples.

Another important aspect to be studied concerns the influence of a nuisance peak. In the following simulations the frequency separation between peak 1 and peak 2 is varied from 20 to 200 Hz. For small peak separations, peak 2 is partly included in the original Interval II. To avoid this the upper bound is modified in this particular case so that Interval II stretches from −141 to 39 Hz instead. The results for the amplitude estimates are shown in Fig. 4. Note that the numerical results on the estimation accuracy presented in Figs. 1–3 correspond to a peak separation of 80 Hz, which appears to be the optimal separation for ERF-HSVD. Hence the scenario considered in Figs. 1–3 was the most favorable one for ERF-HSVD. In other scenarios, ERF-HSVD is significantly outperformed by SELF-SVD. Indeed, we can see from Fig. 4 that SELF-SVD gives satisfying parameter estimates even when the interference from the out of bound component is strong, whereas the parameter estimates of ERF-HSVD are severely affected by the nuisance peak. The influence of nuisance peaks cannot be disregarded in practical NMR applications. Hence ERF-HSVD may be a poor choice for such applications.

Table 1
Required number of flops for the three methods for Interval I and Interval II

| Method | Flops | |
|---|---|---|
| | Interval I | Interval II |
| SELF-SVD | $7.2 \times 10^5$ | $3.3 \times 10^7$ |
| ERF-HSVD | $7.4 \times 10^4$ | $8.1 \times 10^6$ |
| HSVD | $7.4 \times 10^8$ | $7.4 \times 10^8$ |

Finally, as we pointed out previously, it is important to show how the choice of frequency interval affects the resulting parameter estimates. In the 3D surface plots in Fig. 5 $k_1$ is varied from −22 to 8 (−43 to 16 Hz) and $k_M$ is varied from 12 to 42 (23 to 82 Hz). As can be seen, ERF-HSVD gives satisfactory performance only if the frequency interval is "suitably chosen." Since usually this is not possible the concluding remark is that SELF-SVD outperforms ERF-HSVD in terms of robustness.

### 3.2. Real-life data

In this subsection we test our SELF-SVD method on in vitro data. The data set is taken from a standard GE spectroscopic phantom with a low-concentration additional GABA solution. The phantom contains 12.5 mM NAA, 10.0 mM Cr, 3.0 mM Ch, 7.5 mM mI, 12.5 mM Glu, 5 mM lactate, and 0.5 mM GABA. The spectral bandwidth is 2500 Hz and $N$ is 1536. A FFT spectrum of the data along with the selected lower and upper frequency bounds are shown in Fig. 6. We assume that we are specifically interested in estimating the parameters of the choline peak which is located at about −50 Hz (see Fig. 6a).

The selected frequency interval for SELF-SVD and ERF-HSVD is presented in Fig. 6b. The lower and upper frequency bounds (corresponding to $k_1$ and $k_M$) are set to about −60 and −42 Hz, respectively. This interval corresponds to $\frac{1}{128}$ of the total number of data samples $N$

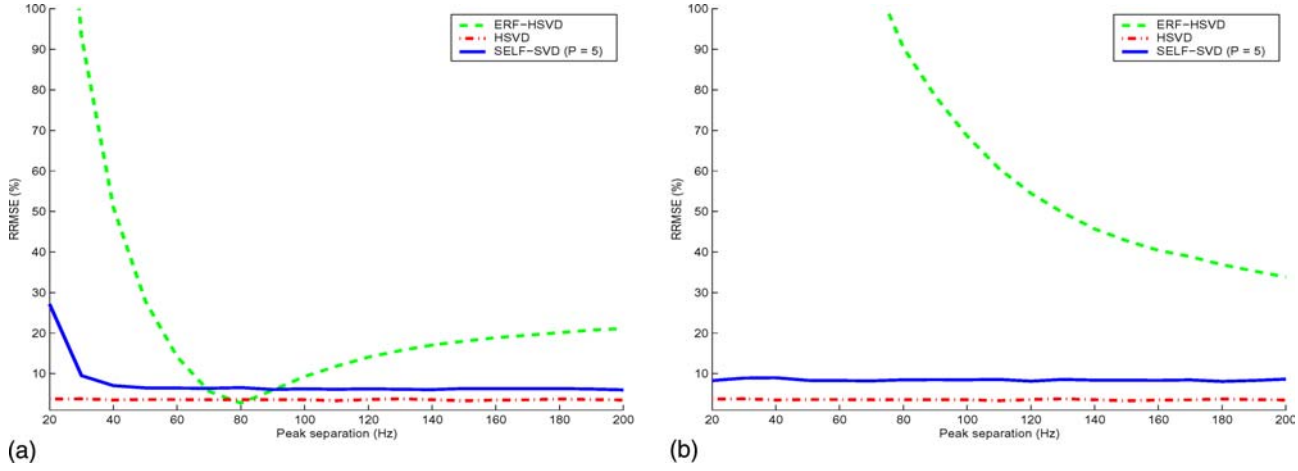


Fig. 4. Amplitude RRMSEs of peak 1 as a function of the frequency separation between peak 1 and peak 2 in the two-peak example: (a) Interval I; (b) Interval II (modified).

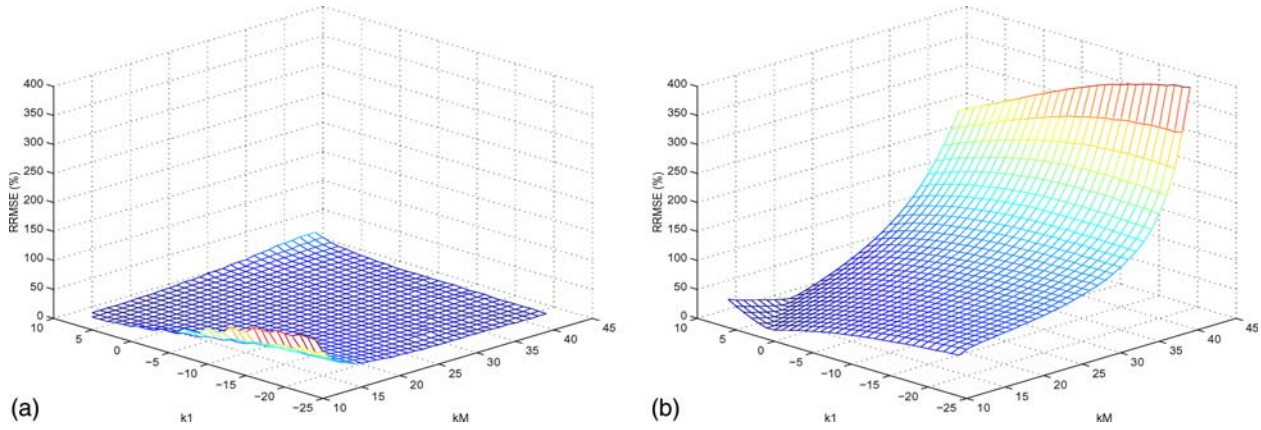


Fig. 5. Amplitude RRMSEs of peak 1 as a function of the lower and upper bounds ($k_1$, respectively, $k_M$) in the two-peak example: (a) SELF-SVD; (b) ERF-HSVD.

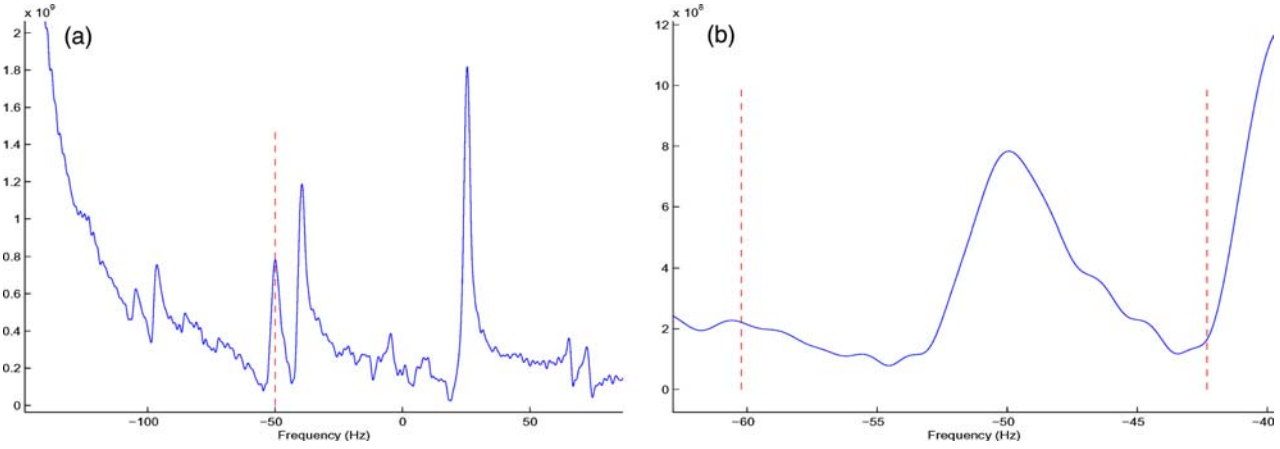


Fig. 6. Magnitude spectrum of in-vitro data and zoom of the choline peak: (a) selected peak of interest; (b) considered frequency interval.

(i.e., $M = 12$ and $S = 4$). Here we choose $P = \lceil N/200 \rceil$ for the amplitude estimation step in SELF-SVD.

The estimates of the three parameters ($\omega$, $\alpha$, $|\rho|$) are shown in Table 2. Assuming that the noise level is fairly low in this data the results of HSVD are here considered as "true values" since the exact parameters are unknown in this case. As can be seen from the table the estimates obtained with SELF-SVD are (much) closer to the HSVD estimates than those given by ERF-HSVD. In fact, the frequency and amplitude estimates obtained with HSVD and SELF-SVD are almost identical. In addition, the last column of the table shows the required number of flops for computing the parameter estimates. The difference between the required flops for HSVD and the other two methods clearly underlines the gain obtained by using a frequency selective approach.

Table 2
Parameter estimates of the choline peak in the in vitro data for the three methods, and the required number of flops

| Method | Freq. ($\omega$) | Damp ($\alpha$) | Ampl $\lvert\rho\rvert$ | No. of flops |
|---|---|---|---|---|
| HSVD | −50.3403 | 7.9011 | $2.3494 \times 10^6$ | $1.9 \times 10^{10}$ |
| SELF-SVD | −50.3565 | 8.2622 | $2.3634 \times 10^6$ | $2.6 \times 10^6$ |
| ERF-HSVD | −49.6796 | 7.0505 | $1.8974 \times 10^6$ | $2.9 \times 10^5$ |

## Acknowledgments

L.V.H. and S.V.H. were supported by interdisciplinary research grants of the research council of the Katholieke Universiteit Leuven, Belgium (IDO/99/03 and IDO/02/09 Project), by the Belgian Programme on Interuniversity Poles of Attraction (IUAP Phase V-22), by the Concerted Action Project MEFISTO-666 of the Flemish Community, and the FWO Projects G.0269.02, G.0270.02, and G.078.01. L.V.H. is a postdoctoral researcher of the FWO (Fund for Scientific Research, Flanders).

We are grateful to Dr. Elfar Adalsteinsson and Dr. Tomas Sundin for providing us with the in vitro data used in the numerical examples section.

## Appendix A. Proof of (11)

First we write the data vector $\mathbf{y}$ as:

$$\mathbf{y} = \sum_{l=1}^{m} \rho_l \mathbf{b}(\lambda_l) + \epsilon. \tag{A.1}$$

Next we note that (for $p = 1, \ldots, S$)

$$\begin{aligned} w_k^p[\mathbf{v}_k^* \mathbf{b}(\lambda)] &= \sum_{t=0}^{N-1} \mathrm{e}^{[-\alpha + \mathrm{i}(\omega - (2\pi/N)k)]t} \mathrm{e}^{\mathrm{i}2\pi kp/N} \\ &= \lambda^p \sum_{t=0}^{N-1} \mathrm{e}^{[-\alpha + \mathrm{i}(\omega - (2\pi/N)k)](t-p)} \\ &= \lambda^p [\mathbf{v}_k^* \mathbf{b}(\lambda)] + \lambda^p \\ &\quad \times \left[ \sum_{t=0}^{p-1} \lambda^{t-p} \mathrm{e}^{-\mathrm{i}2\pi k(t-p)/N} - \sum_{t=N}^{N+p-1} \lambda^{t-p} \mathrm{e}^{-\mathrm{i}2\pi k(t-p)/N} \right] \\ &= \lambda^p [\mathbf{v}_k^* \mathbf{b}(\lambda)] + \lambda^p \sum_{l=1}^{p} \left[ \lambda^{-l} \mathrm{e}^{\mathrm{i}2\pi kl/N} - \lambda^{N-l} \mathrm{e}^{\mathrm{i}2\pi kl/N} \right] \\ &= \lambda^p [\mathbf{v}_k^* \mathbf{b}(\lambda)] + \sum_{l=1}^{p} \lambda^{p-l} (1 - \lambda^N) w_k^l. \end{aligned} \tag{A.2}$$

Let (for $p = 1, \ldots, S$)

$$\gamma_p^*(\lambda) = (1 - \lambda^N) \left[ \lambda^{p-1} \cdots \lambda \ 1 \ 0 \cdots 0 \right] \quad (S \times 1). \tag{A.3}$$

Using this notation we can rewrite Eq. (A.2) in the following more compact form (for $p = 1, \ldots, S$):

$$w_k^p[\mathbf{v}_k^* \mathbf{b}(\lambda)] = \lambda^p [\mathbf{v}_k^* \mathbf{b}(\lambda)] + \gamma_p^*(\lambda) \mathbf{u}_k \tag{A.4}$$

or, equivalently,

$$\mathbf{u}_k [\mathbf{v}_k^* \mathbf{b}(\lambda)] = \mathbf{a}(\lambda) [\mathbf{v}_k^* \mathbf{b}(\lambda)] + \begin{bmatrix} \gamma_1^*(\lambda) \\ \vdots \\ \gamma_S^*(\lambda) \end{bmatrix} \mathbf{u}_k. \tag{A.5}$$

From Eqs. (A.1) and (A.5) it follows that:

$$\begin{aligned} \mathbf{u}_k Y_k &= \sum_{l=1}^{m} \rho_l \mathbf{u}_k [\mathbf{v}_k^* \mathbf{b}(\lambda_l)] + \mathbf{u}_k \varepsilon_k \\ &= [\mathbf{a}(\lambda_1) \ldots \mathbf{a}(\lambda_m)] \begin{bmatrix} \rho_1 \mathbf{v}_k^* \mathbf{b}(\lambda_1) \\ \vdots \\ \rho_m \mathbf{v}_k^* \mathbf{b}(\lambda_m) \end{bmatrix} \\ &\quad + \left\{ \sum_{l=1}^{m} \rho_l \begin{bmatrix} \gamma_1^*(\lambda_l) \\ \vdots \\ \gamma_S^*(\lambda_l) \end{bmatrix} \right\} \mathbf{u}_k + \mathbf{u}_k \varepsilon_k, \end{aligned} \tag{A.6}$$

which proves Eq. (11) (note that the definition of the matrix $\mathbf{\Gamma}$ in Eq. (11) follows from Eq. (A.6), but as we already said this definition is of no interest for the present discussion).

## References


[1] S. Van Huffel, D. van Ormondt, Subspace-based exponential data modeling using prior knowledge, in: Proceedings Signal Processing Symposium, IEEE Benelux Signal Processing Chapter (SPS 98), Leuven, Belgium, March 1998, pp. 211–214.

[2] P. Stoica, Y. Selén, N. Sandgren, S. Van Huffel, Using a priori knowledge in SVD-based NMR spectroscopy – The ATP example, IEEE Trans. Biomed. Eng. (2003), submitted.

[3] L. Vanhamme, T. Sundin, P. Van Hecke, S. Van Huffel, R. Pintelon, Frequency-selective quantification of biomedical magnetic resonance spectroscopy data, J. Magn. Reson. 143 (1) (2000) 1–16.

[4] I. Dologlou, S. Van Huffel, D. van Ormondt, Frequency-selective MRS data quantification with frequency prior knowledge, J. Magn. Reson. 130 (2) (1998) 238–243.

[5] R. Romano, A. Motta, S. Camassa, C. Pagano, M.T. Santini, P.L. Indovina, A new time-domain frequency-selective quantification algorithm, J. Magn. Reson. 155 (2) (2002) 226–235.

[6] S. Cavassila, B. Fenet, A. van den Boogaart, C. Rémy, C. Briguet, D. Graveron-Demilly, ER-Filter: a preprocessing technique to improve the performance of SVD-based quantitation methods, J. Magn. Reson. Anal. 3 (1997) 87–92.

[7] J. Tang, J.R. Norris, LP-ZOOM, a linear prediction method for local spectral analysis of NMR signals, J. Magn. Reson. 79 (1988) 190–196.

[8] J. Slotboom, C. Boesch, R. Kreis, Versatile frequency domain fitting using time domain models and prior knowledge, Magn. Reson. Med. 39 (1998) 899–911.

[9] T. McKelvey, M. Viberg, A robust frequency domain subspace algorithm for multi-component harmonic retrieval, in: Proceedings of the 35th Asilomar Conference on Signals, Systems and Computers, November 2001, pp. 68–72.

[10] P. Stoica, R. Moses, Introduction to Spectral Analysis, Prentice-Hall, Upper Saddle River, NJ, 1997.

[11] S. Van Huffel, J. Vandewalle, The Total Least Squares Problem: Computational Aspects and Analysis, in: Frontiers in Applied Mathematics Series, vol. 9, SIAM, Philadelphia, 1991.

[12] P. Stoica, T. Sundin, Nonparametric NMR spectroscopy, J. Magn. Reson. 152 (2001) 57–69.

[13] H. Barkhuysen, R. de Beer, D. van Ormondt, Improved algorithm for noniterative time-domain model fitting to exponentially damped magnetic resonance signals, J. Magn. Reson. 73 (1987) 553–557.

[14] P. Stoica, H. Li, J. Li, Amplitude estimation of sinusoidal signals: survey, new results and an application, IEEE Trans. Signal Process. 48 (2000) 338–352.

[15] H. Hu, Q.N. Van, V.A. Mandelshtam, A.J. Shaka, Reference deconvolution, phase correction, and line listing of NMR spectra by the 1D filter diagonalization method, J. Magn. Reson. 134 (1998) 76–87.

[16] V.A. Mandelshtam, FDM: the filter diagonalization method for data processing in NMR experiments, Prog. NMR Spectrosc. 38 (2001) 159–196.

[17] Y. Hua, T.K. Sarkar, Matrix pencil method for estimating parameters of exponentially damped/undamped sinusoids in noise, IEEE Trans. ASSP 38 (1990) 814–824.

[18] Y. Hua, T.K. Sarkar, On SVD for estimating generalized eigenvalues of singular matrix pencil in noise, IEEE Trans. SP 39 (1991) 892–900.

[19] S.Y. Kung, K.S. Arun, B. Rao, State space and singular value decomposition based on approximation methods for harmonic retrieval, J. Opt. Soc. Am. (1983) 1799–1811.